DECISION FEEDBACK EQUALIZER DESIGN FOR INSENSITIVITY TO DECISION DELAY

William J. Hillery, Michael D. Zoltowski *

Purdue University
School of Electrical and Computer Engineering
1285 Electrical Engineering Building
West Lafayette, IN 47907

Mark Fimoff

Zenith Electronics Corporation
2000 Millbrook Drive
Lincolnshire, IL 60069

ABSTRACT

In this paper, we use an alternative approach to derive the minimum mean-square error decision feedback equalizer. This derivation yields insight which allows the equalizer to be designed so that its SINR performance is relatively insensitive to variations in the decision delay (also known as the cursor). The design, while generally applicable to the DFE, is illustrated using 8-level vestigial sideband modulation as used in the ATSC digital television standard. We simulate several channels and show that the SINR varies little across a relatively wide band of decision delays.

1. INTRODUCTION

When a decision feedback equalizer (DFE) is used in a communication system, the decision delay, or cursor, is set relative to the start of the training sequence once it is has been detected by the correlator. Over time, the location of the tap energy within the impulse response of the channel will change and the optimum decision delay will also change. In [1], a detailed analysis of the finite-length minimum mean-square error (MMSE) DFE was presented including a method for calculating the optimum decision delay for a given channel. Rather than attempting to track this optimum delay with time, in this paper we investigate the variation in the performance of the DFE as a function of the decision delay and attempt to find a region which is relatively insensitive to the decision delay. Our derivation uses an approach similar to that used in [2, 3] and yields insight into how to choose the decision delay so that the equalizer performance varies little over a fairly wide band of delays. We illustrate this result by simulating the performance of the DFE as the decision delay varies for several channels.

2. SIGNAL MODEL

A model for the received signal is given in Fig. 1 where we have assumed symbol rate sampling. The received signal $z[k]$ is given by

$$z[k] = I[k] * c[k] * q[k] + n[k] * q[k], \tag{1}$$

where $I[k]$ is the transmitted symbol sequence, $c[k]$ is the discrete-time channel including the effect of the transmitted pulse shape, $q[k]$ is matched to the transmitted pulse shape, and $n[k]$ is complex additive white Gaussian noise (AWGN) with variance N_0.

*This research was supported by the National Science Foundation under Grant no. CCR-0118842 and also by the Zenith Electronics Corporation.

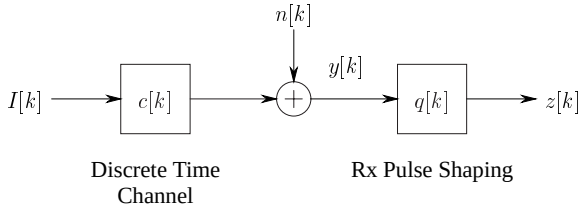

Fig. 1. Discrete time signal model.

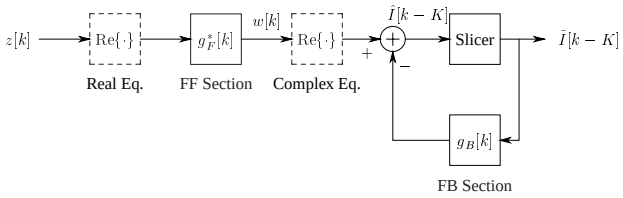

Fig. 2. MMSE DFE block diagram.

The symbol sequence $I[k]$ is assumed to be uncorrelated with zero mean and variance $\mathcal{E}_I = \mathrm{E}\{|I[k]|^2\}$. Define $h[k] = c[k] * q[k]$ and $\nu[k] = n[k] * q[k]$ so that

$$z[k] = I[k] * h[k] + \nu[k], \tag{2}$$

where $\nu[k]$ is colored Gaussian noise.

We assume that the composite channel $h[k]$ has a finite length and is given by the vector $\boldsymbol{h} = [\, h[0] \ \ldots \ h[L_h] \,]^T$. The matched filter $q[k]$ is also finite length and is given by the vector $\boldsymbol{q} = [\, q[-L_q] \ \ldots \ q[0] \ \ldots \ q[L_q] \,]^T$.

3. MMSE DFE DERIVATION

A block diagram of the MMSE DFE is shown in Fig. 2. Since we will illustrate our results using 8-level vestigial sideband modulation (8-VSB) where the constellation is real, the real part of signal is taken prior to subtracting the output of the feedback (FB) section. If the real part is taken before the feedforward (FF) section, the equalizer is entirely real; if taken after the FF section, the FF filter taps are complex-valued. The equalizer derivation assumes a complex FF filter, but it is easily modified for the real case. In addition, it is straightforward to generalize to the case of a fully

complex equalizer (complex-valued FF and FB taps), which is appropriate for a constellation of complex symbols.

The DFE will be derived in three steps. In the first step, we derive an expression for $\boldsymbol{z}[k]$ (the contents of the FF filter delay line) in terms of the desired symbol, past symbols, and future symbols. Second, we subtract the contribution to $\boldsymbol{z}[k]$ from past symbols. Finally, we derive the linear MMSE estimate of the desired symbol from the remaining portion of $\boldsymbol{z}[k]$. Although the derivation does not explicitly assume the structure given in Fig. 2, the structure will follow as an implementation of the resulting expressions. Throughout the derivation, we adopt the convention that a subscript R identifies the real part of a quantity and a subscript I identifies the imaginary part.

We assume that the FF filter $g_F[k]$ has $N_{FF}+1$ taps. The FF filter then acts on $N_{FF}+1$ consecutive samples of the received sequence $z[k]$, which we assemble into a vector $\boldsymbol{z}[k] = [\, z[k] \ \ldots \ z[k-N_{FF}] \,]^T$. Then

$$\boldsymbol{z}[k] = \boldsymbol{H}\boldsymbol{I}[k] + \boldsymbol{\nu}[k], \tag{3}$$

where $\boldsymbol{I}[k] = [\, I[k] \ \ldots \ I[k-L_h-N_{FF}] \,]^T$,

$$\boldsymbol{H} = \begin{bmatrix} \boldsymbol{h}^T & 0 & \cdots & 0 \\ 0 & \boldsymbol{h}^T & \cdots & 0 \\ \vdots & \vdots & \ddots & \vdots \\ 0 & 0 & \cdots & \boldsymbol{h}^T \end{bmatrix}, \tag{4}$$

and $\boldsymbol{\nu}[k] = [\, \nu[k] \ \ldots \ \nu[k-N_{FF}] \,]^T$. The dimensions of the channel matrix $\boldsymbol{H}$ are $(N_{FF}+1) \times (N_{FF}+L_h+1)$.

The colored noise vector is given by

$$\boldsymbol{\nu}[k] \quad = \quad \boldsymbol{Q}\boldsymbol{n}[k], \tag{5}$$

where $\boldsymbol{n}[k] = [\, n[k+L_q] \ \ldots \ n[k] \ \ldots \ n[k-L_q-N_{FF}] \,]^T$ and

$$\boldsymbol{Q} = \begin{bmatrix} \boldsymbol{q}^T & 0 & \cdots & 0 \\ 0 & \boldsymbol{q}^T & \cdots & 0 \\ \vdots & \vdots & \ddots & \vdots \\ 0 & 0 & \cdots & \boldsymbol{q}^T \end{bmatrix}. \tag{6}$$

The dimensions of the pulse matrix $\boldsymbol{Q}$ are $(N_{FF}+1) \times (N_{FF}+2L_q+1)$.

We assume that we are estimating the symbol $I[k-K]$, where K is an integer, known as the decision delay or cursor, whose role is simply to choose the symbol being estimated. As pointed out in [1], the choice of K affects the performance of the equalizer so this is an important design choice. Examination of Eq. 3 indicates that K must satisfy $0 \le K \le L_h + N_{FF}$; otherwise, there is no information about the desired symbol in $\boldsymbol{z}[k]$. The vector $\boldsymbol{I}[k]$ can now be written as

$$\boldsymbol{I}[k] = \begin{bmatrix} \boldsymbol{I}_F[k]^T & I[k-K] & \boldsymbol{I}_P[k]^T \end{bmatrix}^T, \tag{7}$$

where $\boldsymbol{I}_F[k] = [\, I[k] \ \ldots \ I[k+1-K] \,]^T$ contains future symbols and $\boldsymbol{I}_P[k] = [\, I[k-1-K] \ \ldots \ I[k-L_h-N_{FF}] \,]^T$ contains past symbols, relative to the desired symbol. Let the channel matrix be partitioned in a manner compatible with $\boldsymbol{I}[k]$:

$$\boldsymbol{H} = \begin{bmatrix} \boldsymbol{H}_F & \boldsymbol{h}^{(rt)} & \boldsymbol{H}_P \end{bmatrix}. \tag{8}$$

Then Eq. 3 becomes

$$\boldsymbol{z}[k] = \boldsymbol{H}_F\boldsymbol{I}_F[k] + \boldsymbol{h}^{(rt)}I[k-K] + \boldsymbol{H}_P\boldsymbol{I}_P[k] + \boldsymbol{\nu}[k] \tag{9}$$

and the first step of the derivation is complete.

Using Eq. 9, the second step is straightforward. Subtracting from $\boldsymbol{z}[k]$ the contribution from past symbols yields

$$\boldsymbol{z}[k] - \boldsymbol{H}_P\boldsymbol{I}_P[k] = \boldsymbol{H}_f\boldsymbol{I}_f[k] + \boldsymbol{\nu}[k], \tag{10}$$

where $\boldsymbol{I}_f[k] = \begin{bmatrix} \boldsymbol{I}_F[k]^T \ I[k-K] \end{bmatrix}^T$ and $\boldsymbol{H}_f = \begin{bmatrix} \boldsymbol{H}_F \ \boldsymbol{h}^{(rt)} \end{bmatrix}$.

In the final step of the derivation, we estimate the desired symbol using the real part of a linear combination of the elements in $\boldsymbol{z}[k] - \boldsymbol{H}_P\boldsymbol{I}_P[k]$:

$$\begin{aligned} \hat{I}[k-K] \quad &= \quad \mathrm{Re}\{\boldsymbol{g}_F^H\,(\boldsymbol{z}[k] - \boldsymbol{H}_P\boldsymbol{I}_P[k])\} \\ &= \quad \boldsymbol{g}_{FC}^T\,(\boldsymbol{H}_{fC}\boldsymbol{I}_f[k] + \boldsymbol{\nu}_C[k])\,, \end{aligned} \tag{11}$$

where $\boldsymbol{g}_{FC} = \begin{bmatrix} \boldsymbol{g}_{FR}^T \ \boldsymbol{g}_{FI}^T \end{bmatrix}$, $\boldsymbol{\nu}_C[k] = \begin{bmatrix} \boldsymbol{\nu}_R^T[k] \ \boldsymbol{\nu}_I^T[k] \end{bmatrix}$, and

$$\boldsymbol{H}_{fC} = \begin{bmatrix} \boldsymbol{H}_{fR} \\ \boldsymbol{H}_{fI} \end{bmatrix}. \tag{12}$$

The MMSE linear FF filter can then be found using the principal of orthogonality which states that

$$\mathrm{E}\left\{ \left(I[k-K] - \hat{I}[k-K] \right) (\boldsymbol{H}_{fC}\boldsymbol{I}_f[k] + \boldsymbol{\nu}_C[k]) \right\} = 0. \tag{13}$$

Then

$$\left(\boldsymbol{H}_{fC}\boldsymbol{H}_{fC}^T + \frac{1}{\mathcal{E}_I}\boldsymbol{R}_{\nu_C\nu_C} \right) \boldsymbol{g}_{FC} = \boldsymbol{h}_C^{(rt)}, \tag{14}$$

where $\boldsymbol{h}_C^{(rt)} = \begin{bmatrix} \boldsymbol{h}_R^{(rt)T} \ \boldsymbol{h}_I^{(rt)T} \end{bmatrix}^T$,

$$\boldsymbol{R}_{\nu_C\nu_C} = N_0\boldsymbol{P}_C = N_0 \begin{bmatrix} \boldsymbol{P}_R & -\boldsymbol{P}_I \\ \boldsymbol{P}_I & \boldsymbol{P}_R \end{bmatrix}, \tag{15}$$

and $\boldsymbol{P}_R$ and $\boldsymbol{P}_I$ are Toeplitz matrices containing, respectively, samples of the real and imaginary parts of the time autocorrelation of the matched filter.

From Eq. 11, we can now see that the DFE can be implemented using the structure in Fig. 2 by noting that

$$w_R[k] = \mathrm{Re}\{\boldsymbol{g}_F^H\boldsymbol{z}[k]\}. \tag{16}$$

Then the FB filter $\boldsymbol{g}_B = [\, g_B[1] \ \ldots \ g_B[N_{FB}] \,]^T$ is given by $\boldsymbol{g}_B = \mathrm{Re}\{\boldsymbol{H}_P^H\boldsymbol{g}_F\}$, which simplifies to

$$\boldsymbol{g}_B = \boldsymbol{H}_{PC}^T\boldsymbol{g}_{FC}, \tag{17}$$

where $\boldsymbol{H}_{PC} = \begin{bmatrix} \boldsymbol{H}_{PR} \\ \boldsymbol{H}_{PI} \end{bmatrix}$. Due to the dimensions of the matrix $\boldsymbol{H}_{PC}$, the number of FB taps N_{FB} is restricted to

$$N_{FB} = L_h + N_{FF} - K. \tag{18}$$

It is this restriction alone which causes the this derivation of the DFE to be less general than the finite length complex MMSE DFE derived in [4], although they are equivalent under this restriction.

In Eq. 11, the contribution from the desired symbol to the symbol estimate is $\boldsymbol{g}_{FC}^H \boldsymbol{h}_C^{(rt)} I[k-K]$. So the FF filter combines the energy available from $I[k-K]$ in $\boldsymbol{z}[k]$. It is important to note that at the same time the FF filter attempts to cancel the contribution from $\boldsymbol{I}_F[k]$ balancing against noise enhancement. In order to include all of the energy from $I[k-K]$ in $\hat{I}[k-K]$, $\boldsymbol{h}_C^{(rt)}$ should contain the entire channel response. Therefore, $N_{FF} \geq L_h$ and $L_h \leq K \leq N_{FF}$. The channel length may vary from channel to channel so we choose $N_{FF} = L_{h,max}$, the maximum channel length, and K is nominally $L_{h,max}$. Since the initial and final portion of the channel response contains the tails of the pulse shape — at least $2L_q$ samples at each end — and these samples generally contain little energy, K may vary from its nominal value without losing a significant amount of energy from the desired symbol as long as the variation is less than $\pm 2L_q$. In fact, from this perspective the equalizer performance should be changing gradually for $k_0 + d_{max} \leq K \leq N_{FF} + k_0 + d_{min}$, where k_0 is the index of the reference "zero" delay path, and d_{min} and d_{max} are the relative delays the minimum delay path and the maximum delay path. For $N_{FF} + k_0 + d_{min} \leq K \leq N_{FF} + k_0 + d_{max}$ and $k_0 + d_{min} \leq K \leq k_0 + d_{max}$, the performance is likely to drop more quickly since, in this range, the energy contributed by the channel paths is dropping out of the symbol estimate. Outside these regions, the only remaining contribution from $I[k-K]$ is due to the pulse tails so the performance should drop quickly.

4. SIMULATION RESULTS

In all of the simulations, an 8-VSB system is simulated and the channel is assumed to be known. The complex pulse shape at the transmitter and receiver each have a square-root raised cosine spectrum designed for one-half the symbol rate but shifted up in frequency by one-fourth of the symbol rate. The excess bandwidth is 0.115 and $L_q = 30$. All simulations are performed at a received SNR of 20 dB. Both complex and real equalizers are simulated.

We first simulate a simple multipath channel which completely fills the number of taps allotted; that is, $k_0 + d_{min} = 2L_q$ and $k_0 + d_{max} = L_{h,max} - 2L_q$. Channel 1 contains paths at relative delays of -10 (d_{min}), 0, and 30 (d_{max}) symbols with respective real gains of 0.3, 1.0, and 0.5 and $k_0 = 70$. In addition, the same channel is simulated again with randomly generated complex phases of 127°, 55°, and -116°, respectively. The channel length L_h is 160, so $N_{FF} = 160$. The decision delay K is varied from 10 to 310 in steps of 10. The number of FB taps is given by Eq. 18. Figure 3 contains a plot of the cumulative energy in the channel as a fraction of the total energy. The cumulative energy is the norm of $[\, h[0] \ldots h[k] \,]^T$ divided by $\|\boldsymbol{h}\|^2$. In both the real and complex channels, most of the energy in each path is heavily concentrated near the center of its pulse so the plot looks like a stairstep function with transitions at the path delays ($k_0 + d_i$, for relative delay d_i). With complex gains, both curves look like the plot of the complex channel in Fig. 3. Figure 4 shows the variation in SINR as a function of decision delay for real path gains. Results for complex path gains are shown in Fig. 5 In each case, the center marker (dotted line) in the plot is placed at $K = N_{FF}$, the two neighboring markers (dotted) are placed at $N_{FF} \pm 2L_q$, and the outer markers (dash-dot) are placed at $2L_q$ and $N_{FF} + L_h - 2L_q$. In each case, the SINR varies by a fraction of a dB across the inner range and begins dropping outside this range since significant channel energy begin to fall outside of the symbol estimate as the path delay points drop out of $\boldsymbol{h}^{(rt)}$. The performance drops even more dramatically

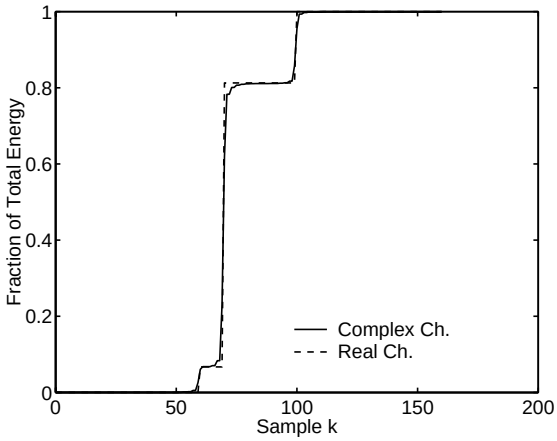

Fig. 3. Cumulative channel energy for Channel 1 with real gains.

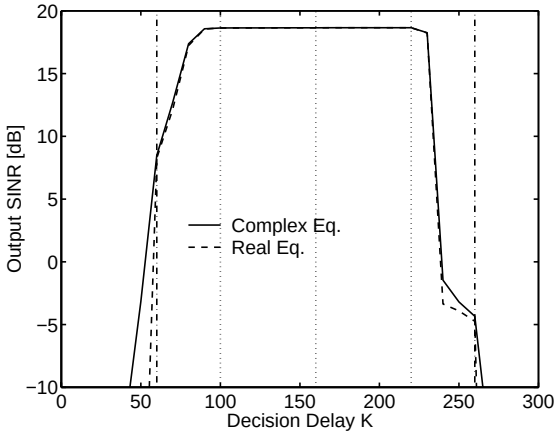

Fig. 4. SINR at the equalizer output for Channel 1 with real gains at an input SNR of 20 dB.

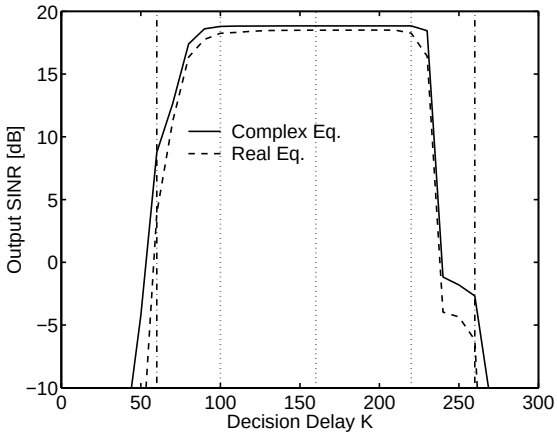

Fig. 5. SINR at the equalizer output for Channel 1 with complex gains at an input SNR of 20 dB.

Table 1. Brazil D and ATTC C channel characteristics

Brazil D		ATTC C	
Delay	**Gain**	**Delay**	**Gain**
0	1.0	-19.0	0.13
5.2	0.66	0	1.0
22.3	0.76	1.6	0.10
31.2	0.87	19.0	0.10
61.5	1.02	60.3	0.32
62.2	0.74	190.3	0.20

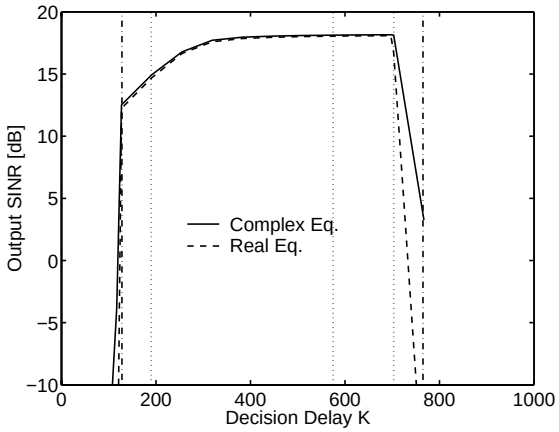

Fig. 6. SINR at the equalizer output for Brazil D at an input SNR of 20 dB.

outside the outer range. The inner range provides a relatively wide band of delays where the SINR is relatively constant.

The second pair of channels, Brazil D [5] and ATTC C [6] have delays and gains given in Table 1. The phase of each path gain was set to $2\pi f_c T_s d_i$ where f_c is a carrier frequency of $50\mathrm{MHz}$, T_s is the symbol period ($91.9\mathrm{ns}$), and d_i is the relative path delay. In both of the cases, $L_h = N_{FF} = 575$ and K is varied from 63 to 1087 in steps of 64 with additional points from 77 to 117 and from 647 to 697 in steps of 10. The results are shown in Figs. 6 and 7. In both channels, delay zero was located in channel tap $k_0 = 127$. As before, the center (dotted) marker in the plot is placed at $K = N_{FF}$. Since the channel vectors have zero values at both ends, the inner (dotted) markers are at $k_0 + d_{max}$ and $N_{FF} + k_0 + d_{min}$; the outer (dash-dot) markers are at $k_0 + d_{min}$ and $N_{FF} + k_0 + d_{max}$. We see that the SINR is near its peak when $K = N_{FF}$ and that there is little variation in SINR over much of the inner band. In Brazil D, there is a gradual drop in the SINR for $K < N_{FF}$ but the drop does not exceed 1.7 dB until K is within $2L_q$ of the edge of the inner region. The drop is likely related to the large gains of the paths with delays of 61.5 and 62.2 symbols, but the mechanism is somewhat more complicated than described here because the channel energy loss in this region is quite small. At the upper end of the inner band, the SINR of the equalizer is nearly constant until the edge of the band in both channels. Outside the inner band, the performance loss, when it occurs, is more dramatic, as expected. Even though the performance is not completely constant across the inner range, there is still a relatively wide region of nearly constant performance.

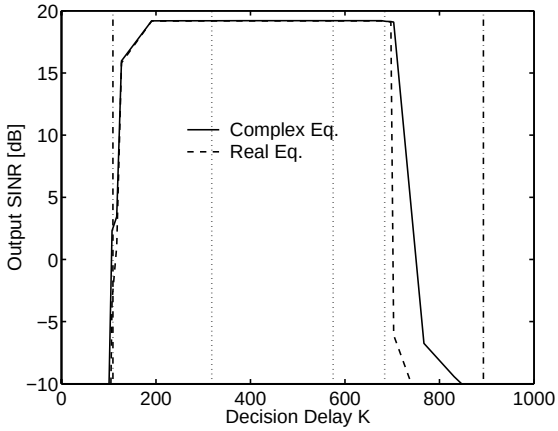

Fig. 7. SINR at the equalizer output for ATTC C with complex gains at an input SNR of 20 dB.

5. CONCLUSIONS

We have shown an alternative derivation for the MMSE DFE which gives insight into how to choose the number of equalizer taps and how to make the performance relatively insensitive to the decision delay. When the number of FF taps is at least as large as the span of the non-zero channel taps (those contributing significant energy to the total channel energy), there is a fairly wide band of decision delays where the SINR is relatively flat. The number of FB taps required was found to depend on the decision delay, but can be fixed at the same number of taps as in the FF filter when N_{FF} is chosen to be the maximum span of the channel taps ($L_{h,max}$).

6. REFERENCES

[1] N. Al-Dhahir and J. M. Cioffi, "MMSE decision-feedback equalizers: Finite-length results," *IEEE Trans. Comm.*, vol. 43, no. 10, pp. 2582–2594, Oct. 1995.

[2] I. J. Fevrier, S. B. Gelfand, and M. P. Fitz, "Reduced complexity decision feedback equalization for multipath channels with large delay spread," *IEEE Trans. Comm.*, vol. 47, no. 6, pp. 927–937, Jun. 1999.

[3] S. Ariyavisitakul and L. J. Greenstein, "Reduced-complexity equalization techniques for broadband wireless channels," *IEEE J. Sel. Area Comm.*, vol. 15, no. 1, pp. 5–15, Jan. 1997.

[4] M. D. Zoltowski, W. J. Hillery, S. Özen, and M. Fimoff, "Conjugate-gradient-based decision feedback equalization with structured channel estimation for digital television," in *Digital Wireless Communications*, Raghuveer M. Rao, Soheil A. Dianat, and Michael D. Zoltowski, Eds., 2002, vol. 4740 of *Proc. of SPIE*, pp. 95–105.

[5] "Teste em sistemas de televisão digital: relatório final," $\mathrm{http://www.anatel.gov.br/biblioteca/publicacao/relatorio\_tvdigital\_cp216.htm}$, 5 Feb. 2000, Section 3.3.

[6] Advanced Television Technology Center, "Evaluation of ATSC 8-VSB receiver performance in the presence of simulated multipath and noise," Document 99-04A, 13 September 1999.